Gain without inversion and enhancement of refractive index via intervalley quantum coherence transfer in hybrid WS_2-metallic nanoantenna systems

Seyed M. Sadeghi [1,*] and Judy Z. Wu [2]

[1]*Department of Physics and Astronomy, University of Alabama in Huntsville, Huntsville, Alabama 35899, USA*

[2]*Department of Physics and Astronomy, University of Kansas, Lawrence, Kansas 66045, USA*

(Received 25 January 2021; accepted 5 April 2021; published 16 April 2021)

We theoretically study formation of gain without inversion and resonant enhancement of refractive index with suppressed absorption in a system consisting of a monolayer of transition metal dichalcogenide (WS_2) and a metallic nanoantenna. We show that these processes happen when the hybrid system interacts with a right-circularly polarized laser beam, allowing quantum coherence transfer to happen from the K to K′ valley. Our results show that the quantum coherence transfer can convert the K′ valley into a conjugated system wherein the real and imaginary parts of its polarization become similar to the imaginary and real parts of the K valley polarization, respectively. This allows the maximum refractive index in the K′ valley to occur as the absorption becomes zero. We characterize the conjugated valley system by inspecting the evolution of its Bloch vector as the incident laser frequency varies. The theoretical approach includes density matrix formalism while considering a pure dephasing rate that represents the fast decay of exciton valley polarization in transition metal dichalcogenide monolayers.

DOI: 10.1103/PhysRevA.103.043713

I. INTRODUCTION

Recently, interaction of monolayers (MLs) of transition metal dichalcogenide (TMD) with localized surface plasmon resonances (LSPRs) of metallic nanoantennas (mANTs) has been investigated intensivel. It has been shown that hybridization of excitons associated with the K and K′ valleys (K-exc and K′-exc) with LSPRs can lead to interesting results. These include generation of coherent intervalley dynamics [1–4], valley Rabi splitting, dressed states, exciton polaritons [5–8], and enhancement of second harmonic generation [9]. Recent reports have also demonstrated control of the absorption and emission of TMD MLs via hot electrons [10], chiral plasmonic hybridization [11], and valley-polarized directional emission [12]. It is shown that interaction of plasmonic spiral rings and TMD MLs allows one to use optical spin states to control the plasmonic emission enhancement [13]. Additionally, interaction of plasmonic chiral metasurfaces with valley-polarized excitons can also support control of the emission spectra of TMD MLs in the far field [14]. Moreover, strong chiral exciton-plasmon coupling in TMD-LSPR systems can be used for spin-selective excitation of directional flow of polaritons [1]. In terms of device applications, recently, hybrid systems consisting of TMD MLs and mANTs have been used for high performance photodetectors [15]. Additionally, superposition of the LSPRs of mANTs with those of WS_2 and MoS_2 nanodomes are used for surface-enhanced Raman spectroscopy with high sensitivities [16,17].

Recently, we showed that when a system consisting of a ML of WS_2 and a mANT interacts with a right-circularly polarized (RCP) (σ_+) laser field [Fig. 1(a)], quantum coherence can be transferred from one valley (K) to another (K′) [18]. A prime impact of this process was shown to be coherently induced handedness and plasmonic control of the valley quantum coherence. The main mechanism behind the quantum coherence transfer in the WS_2-mANT system is formation of plasmonically mediated coherent intervalley coupling. Such a coupling is generated via direct excitation of K-exc and LSPRs by the σ_+ laser field. Although it is not influenced directly by such a field, the K′ valley can be excited coherently by the fields of K-exc and LSPRs, and by their phase-correlated mixing. Under these conditions, polarization and population can be transferred from the K to K′ valley with a given phase relation [18]. The plasmonically mediated coherent intervalley coupling can also lead to coherently driven transfer of energy from the WS_2 ML to the mANT, offering coherent control of plasmon excitations in the mANT.

The intervalley quantum coherence offers a unique way of transfer of not only energy (excitation population) but also polarization and phase from one valley to another. Such a process is different from intervalley carrier relaxation, wherein the valley population transfer occurs via incoherent carrier scattering. The objective of this paper is to show that in a system, as shown in Fig. 1(a), when the K valley is excited by a σ_+ laser field, the intervalley quantum coherence transfer can transform the K′ valley into a quantum conjugated system. In such a system, under certain conditions, the real (imaginary) part of K′-exc behaves as the imaginary (real) part of K-exc. As a result, while the K valley polarization follows its standard features dictated by the intrinsic material properties of the TMD ML, the K′ valley supports gain without inversion (GWI) and resonant refractive index enhancement with zero absorption. These processes happen under quite different

*seyed.sadeghi@uah.edu

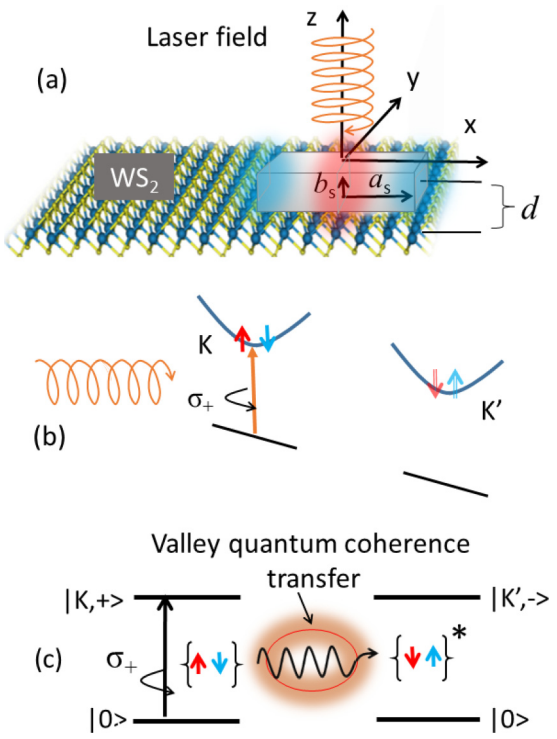

FIG. 1. (a) Schematic illustration of the WS_2-mANT system interacting with a right-circularly polarized laser field (σ_+). (b) Optical excitation with the WS_2 ML via a circularly polarized light. (c) Quantum coherence transfer from K-exc ($|K,+\rangle$) to K′-exc ($|K',-\rangle$) via the plasmons of the mANT. Here $\{\uparrow,\downarrow\}$ and $\{\downarrow,\uparrow\}^*$ refer, respectively, to spin valley state of K valley and the valley conjugate system.

coherent preparation conditions than those adopted for atomic and solid state systems [19–22]. We study the evolution of the Bloch vectors associated with the K and K′ valleys, demonstrating the distinct polarization phase information that each vector can carry at different frequencies of the laser field. The type of GWI predicted in this paper may support efficient transfer of energy from the mANTs to TMD MLs [23]. The results presented in this paper are obtained considering the strong dipolar excitations in mANTs [24] and exciton valley polarization lifetime as short as 400 fs. This is in accord with recent observations of the polarization dephasing rate at room temperature [25–28].

II. THEORY

The system considered in this paper includes a silver (Ag) mANT with a length of $2a_s$ and width and hight of $2b_s$, placed on the surface of a WS_2 ML [Fig. 1(a)]. The center-to-center distance between mANT and the ML is d. The materials surrounding these are assumed to have dielectric constant ε_0. The WS_2-mANT system interacts with a RCP laser field (σ_+), $\mathbf{E} = E_0(t)\cos(\omega t)\hat{\mathbf{e}}_+$. Here ω is the frequency of the laser, $E_0(t)$ is its time-dependent amplitude, and $\hat{\mathbf{e}}_+$ is the polarization unit vector for RCP. To be able to address the plasmon resonances of the mANT analytically, we approximate the shape of the mANT as a spheroid with polarization (γ) given by $\gamma = [\varepsilon_m(\omega) - \varepsilon_0]/[3\varepsilon_0 + 3\kappa(\varepsilon_m(\omega) - \varepsilon_0)]$. Here κ is the depolarization factor of the spheroid when the incident laser field is polarized along a_s, and the dielectric function of the metal (ε_m) includes both interband transition and Drude effects [29].

Interaction of the σ_+ laser with the TMD ML directly excites K-exc. Intervalley quantum coherence transfer, however, can lead to the excitation of K′-exc. To see this, consider $a_+^\dagger$ and $b_-^\dagger$ are the creation operators for K-exc ($|K,+\rangle$) and K′-exc ($|K',-\rangle$), respectively [Fig. 1(c)]. a_0 and b_0, on the other hand, are the annihilation operators for their ground states ($|0\rangle$). μ_+ and μ_- are the dipole moments associated with the σ_+ and σ_- transition components, i.e., K-exc and K′-exc, respectively [Fig. 1(c)]. They are considered to be equal. Under these conditions, the interaction terms for the K and K′ valleys are given by $H_{\rm int}^{K} = -\mu_+ E_K a_+^\dagger a_0 + \text{c.c.}$ and $H_{\rm int}^{K',K} = -\mu_- E_{K',K} b_+^\dagger b_0 + \text{c.c.}$, respectively. Here E_K and $E_{K,K'}$ are the fields experienced by the K and K′ valleys in the presence of the laser field. The former includes direct interaction of the laser field with the K valley ($E_{\rm exc}^+$). Because of the valley selection rules, this term does not exist for the K′ valley. Since the mANT is also excited by the σ_+ field, E_K and $E_{K',K}$ include fields generated by direct excitation of the LSPRs, i.e., $E_{\rm plas}^+$ and $E_{\rm plas}^-$, respectively. The prominent terms in E_K and $E_{K,K'}$, however, are the K-valley self-induced field ($E_{KK}^{\rm plas}$) and K-valley induced field in the K′ valley ($E_{K'K}^{\rm plas}$). These terms are given by the following:

$$E_{KK}^{\rm plas} = GP_K^+\hat{e}_+, \quad E_{K'K}^{\rm plas} = GP_K^+\hat{e}_-, \tag{1}$$

where $G = \frac{S_\alpha^2\gamma a_s b_s^2}{2\varepsilon_{\rm eff}^2 d^6}$ and $P_K^+ = \mu_+\rho_{0,+}^K + \text{c.c.}$ Here $\rho_{0,+}^K$ is the polarization or coherent term of the density matrix of the K valley ($\rho^{\rm K}$). $\varepsilon_{\rm eff} = \varepsilon_{\rm ML}/\varepsilon_0$, wherein $\varepsilon_{\rm ML}$ is the screening dielectric function of the WS_2 ML, representing the external field experienced by K-exc. S_α is a polarization factor determined by the direction of the polarization of the laser field. Since this field propagates perpendicular to the plane of the WS_2 ML, i.e, parallel to the z axis, we have $S_\alpha = -1$.

$E_{K'K}^{\rm plas}$ is the key parameter for transfer of intervalley quantum coherence from the K to K′ valley. Its presence suggests that the density matrix associated with these valleys are, respectively, given by [18]

$$\dot{\rho}^K = -\frac{i}{\hbar}\left[H_0 + H_{\rm int}^K, \rho^K\right] + [L\rho^K]_{\rm damp} \tag{2}$$

and

$$\dot{\rho}^{K',K} = -\frac{i}{\hbar}\left[H_0 + H_{\rm int}^{K',K}, \rho^{K',K}\right] + [L\rho^{K',K}]_{\rm damp}. \tag{3}$$

Here H_0 is the Hamiltonian of the WS_2 ML in the absence of the laser field. A key feature highlighted by these equations is the fact that equation of motion of K′-exc is driven by the K-exciton. This can be seen considering the interaction terms in Eqs. (2) and (3) expressed in the following [18]:

$$H_{\rm int}^K = \hbar\Omega_{\rm nor}^K(\rho)a_+^\dagger a_0 + \text{H.c.} \tag{4}$$

$$H_{\rm int}^{K',K} = \hbar\Omega_{\rm nor}^{K',K}(\rho)b_-^\dagger b_0 + \text{H.c.} \tag{5}$$

Here $\Omega_{\rm nor}^{K(K')}$ refers to the coherently normalized Rabi frequencies of K-exc and K′-exc, given by

$$\Omega_{\rm nor}^{K}(\rho)=\Omega_{\rm eff}^{K}+\eta_{+}\rho_{0,+}^{K},\quad \Omega_{\rm nor}^{K',K}(\rho)=\Omega_{\rm eff}^{K'}+\eta_{+}\rho_{0,+}^{K}. \tag{6}$$

Here $\Omega_{\rm eff}^{K}=\Omega_{0}^{K}(1+\frac{S_\alpha\gamma a_s b_s^2}{d^3})$, $\Omega_{\rm eff}^{K'}=\Omega_{0}^{K'}\frac{S_\alpha\gamma a_s b_s^2}{d^3}$, and $\Omega_{0}^{K(K')}=\frac{\mu_{+(-)}E_0(t)}{2\hbar\varepsilon_{\rm eff}}$ are, respectively, referring to the Rabi frequencies associated with the K and K′ valleys in the presence of pure plasmonic effects (no coherent effects) and in the absence of the mANT. Additionally, in the above equations $\eta_{+}=G\mu_{+}$.

Note that these equations are obtained using $\hat{\mathbf{e}}_{+}=\frac{1}{\sqrt{2}}(\hat{\mathbf{e}}_{\mathbf{x}}+i\hat{\mathbf{e}}_{\mathbf{y}})$, wherein $\hat{\mathbf{e}}_{\mathbf{x}}$ and $\hat{\mathbf{e}}_{\mathbf{y}}$ are polarization units along the x axis and y axis [Fig. 1(a)]. Additionally, we considered the frequency of the laser such that it can only excite the primary longitudinal plasmonic mode of the mANT. $[L\rho^{K}]_{\rm damp}$ and $[L\rho^{K',K}]_{\rm damp}$ in Eqs. (2) and (3) refer to the damping rates of K-exc and K′-exc, respectively, which are introduced in a phenomenological way.

Considering these, the density matrix equations for K′-exc in the WS_2-mANT system have the following forms [30,31]:

$$\dot{\rho}_{0,0}^{K',K}=-2{\rm Im}\big[\Omega_{\rm eff}^{K',K}\rho_{-,0}^{K',K}\big]+\Sigma_{F}^{K',K}+\Gamma\rho_{-,-}^{K',K}, \tag{7}$$

$$\dot{\rho}_{-,-}^{K',K}=2{\rm Im}\big[\Omega_{\rm eff}^{K',K}\rho_{-,0}^{K',K}\big]-\Sigma_{F}^{K',K}-\Gamma\rho_{-,-}^{K',K}. \tag{8}$$

$$\dot{\rho}_{-,0}^{K',K}=-\big[i\Delta_{\rm eff}^{K',K}+\gamma_t\big]\rho_{-,0}^{K',K}-i\Omega_{\rm eff}^{K'}\delta^{K'}. \tag{9}$$

Here $\delta^{K'}=(\rho_{0,0}^{K',K}-\rho_{-,-}^{K',K})$, $\Delta_{\rm eff}^{K',K}$ is the effective detuning of the K′-exc transition from the laser field, and $\gamma_t^{K'}$ is the valley polarization dephasing rate. They are given by

$$\Delta_{\rm eff}^{K',K}=\hbar\omega_{K'}-{\rm Re}[G\mu_{+}]\delta^{K',K}-\hbar\omega\quad \gamma_t^{K'}=\gamma_{0,-}^{K'}+\Lambda_{\rm eff}^{K',K}. \tag{10}$$

Here $\omega_{K'}$ is the frequency of K′-exc and $\Lambda_{\rm eff}^{K',K}={\rm Im}[G\mu_{+}]\delta^{K'}$. $\gamma_{0,-}^{K'}=\Gamma/2+\gamma_p$ is the polarization dephasing rate of the K′-exc in the absence of mANT. Here γ_p refers to the pure dephasing rate of such excitons caused by various processes, including exciton exchange interaction [32–34], scattering with impurities, etc. Γ represents the energy relaxation rate of K′-exc. The term $\Sigma_F^{K',K}$ in Eqs. (7) and (8) refers to the energy transfer from K′-exc to the mANT, generated by intervalley quantum coherent coupling. It is given by $\Sigma_F^{K',K}=2{\rm Im}[G\mu_{+}\rho_{+,0}^{K',K}\rho_{0,-}^{K',K}]$. To obtain the set of equations for K-exc, one needs to replace superscripts K′ with K and subscripts $(-,0)$ with $(+,0)$, and $(-,-)$ with $(+,+)$ [18].

Note that, in general, quantum emitters can interact with each other via dipole-dipole coupling [35,36]. In the formalism presented in this paper, the interaction between the WS_2 ML and the mANT were treated within the dipole-dipole approximation. Since the concentration of the excitons were considered to be low, however, the dipole-dipole interaction between excitons were ignored [37]. When the concentration of the excitons increases, however, the valley polarization decays faster via the stronger impact of the exciton-exciton scattering [32].

III. QUANTUM CONJUGATE VALLEY

For simulation, we consider $\mu_{-}=\mu_{+}=1.12\,e\times$ nm, and the linewidths of K-exc and K′-exc are about 20 meV [7,38]. This corresponds to $\gamma_p^{K(K')}=2.5\,{\rm ps}^{-1}$, approximately depicting room temperature linewidth of emission of WS_2 MLs [38]. The K- and K′-exc transition energy ($\hbar\omega_{K(K')}$) is considered to be 2.006 eV and their radiative lifetimes is assumed to be 1.5 ns [39]. Additionally, for the Ag mANT, we assume $a_s=9$ and $b_s=4$ nm, and $\varepsilon_0=3.61$ (SiN). This leads to a longitudinal plasmon peak very close to $\hbar\omega_K$ and $\hbar\omega_{K'}$. In terms of dielectric constant of the WS_2 ML, we consider $\varepsilon_{\rm ML}\sim 13.7$, which is the static in-plane dielectric constant of the WS_2 ML [40]. The thickness of WS_2 ML has also been shown to be ∼0.6 nm [8]. Note quantum coherence transfer can be limited by the intervalley scattering processes, as they can cause incoherent transfer of population from one valley to another [32,34]. Recent reports have shown the timescales of such processes are between tens of fs to a few ps [32,33]. In the formalism adopted in this paper, we included the impact of such scattering processes in the loss of valley polarization via γ_p. Also note that WS_2 MLs supports two sets of excitons (A and B). The energy difference between these excitons, however, is about 390 meV [41]. The range of variations of the photon energy of the laser considered in this paper is 100 meV, around the central energy of exciton A. Therefore, its interaction with exciton B is insignificant. The following results were obtained considering numerical solutions to Eqs. (7)–(9) under quasi-steady-state conditions.

We start with the results for K-exc. Figure 2 shows variations of the real and imaginary parts of $\rho_{+,0}^{K}$, and the values of $\rho_{+,+}^{K}$ and Σ_F^{K} as a function of the laser frequency [$\Delta_{12}=\hbar(\omega_{K',K}-\omega)$] when the intensity of the incident laser is $45\,{\rm W/cm^2}$ and d is varied. For $d=30$ nm, the impact of the mANT is relatively small and ${\rm Re}[\rho_{+,0}^{K}]$ and ${\rm Im}[\rho_{+,0}^{K}]$ mostly follow the standard features of a driven two-level system [solid lines, Figs. 2(a) and 2(b)]. The results for $d=15$ nm show parts of ${\rm Im}[\rho_{+,0}^{K}]$ becomes negative [Fig. 2(b′), line 1], suggesting GWI. This continues further until the ${\rm Im}[\rho_{21}]$ becomes quite dispersive for $d=10$ and 7 nm [Fig. 2(b′), lines 2 and 3]. These results are similar to those obtained in systems consisting of a quantum dot and a mANT. In Ref. [23], in particular, this process was associated with the transfer of energy from the mANT to the QD. The results in Fig. 2(b′) suggest a much more efficient GWI generation. This is the result of the atomically thick nature of the WS_2 ML and larger dipole moments, which offer a much stronger exciton-plasmon coupling.

The results for $\rho_{+,+}^{K}$ [Figs. 2(c) and 2(c′)] also indicate the expected impact of the near field of the mANT, which increases the excitation rates of K-exc. Σ_F^{K} in Figs. 2(d) and 2(d′) show the rate of the coherently driven energy transfer from the WS_2 ML to the mANT. This rate increases with the decrease of d. Figure 2(d′) indicates that for $d=7$ nm this leads to formation of a doublet (line 3) [18]. A key feature of this process is that it is driven by the quantum coherence. The presence of GWI at certain wavelength range where Σ_F^{K} is significant may suggest exchange of energy between the TMD ML and the mANT.

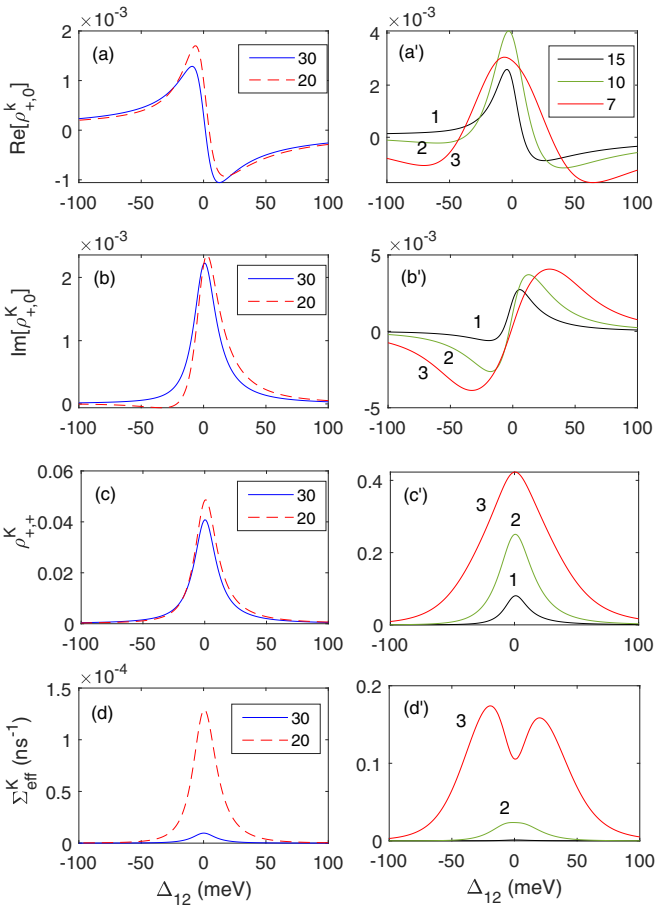

FIG. 2. Variations of the real [(a) and (a′)] and imaginary parts of $\rho^{K}_{+,0}$ [(b) and (b′)], $\rho_{+,+}$ [(c) and (c′)], and Σ^{K}_{F} [(d) and (d′)] as a function of the laser frequency (Δ_{12}). The legends show the values of d. Lines 1, 2, and 3 in (a′)–(d′) refer to $d = 15$, 10, and 7 nm, respectively.

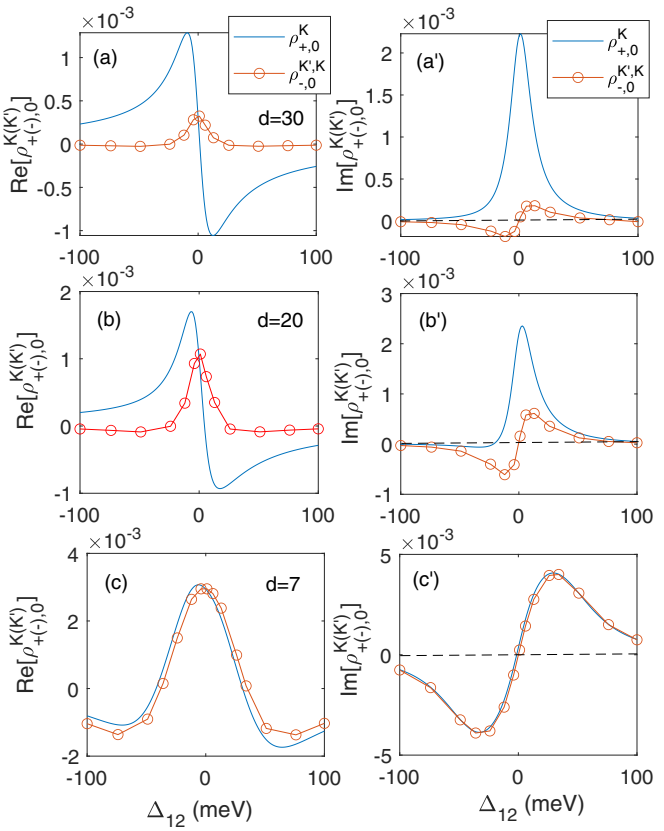

FIG. 3. Variation of the real and imaginary parts of $\rho^{K}_{+,0}$ and $\rho^{K',K}_{-,0}$ as a function of the laser frequency (Δ_{12}) when $d = 30$ [(a) and (a′)], 20 [(b) and (b′)], and 7 nm [(c) and (c′)]. All specifications are the same as those in Fig. 2.

The results presented in Fig. 2 happen via direct interaction of the σ_+ laser field with the K valley. Although such a laser does not directly interact with the K′ valley, the presence of the mANT and formation plasmonic-induced intervalley quantum coherence can transfer polarization and phase to this valley. To see this, Fig. 3 presents the results for Re[$\rho^{K',K}_{-,0}$] [Figs. 3(a)–3(c)], Im[$\rho^{K'}_{-,0}$, K] [Figs. 3(a′)–3(c′)] as a function of Δ_{12} for different values of d (circles). Comparing these results with those associated with $\rho^{K}_{+,0}$ (solid lines) suggests significant differences between the K′ and K valley polarization. For $d = 30$ nm, we can see the real part of K′-exc as a function Δ_{12} is spectrally similar to that of the imaginary part of K-exc [Figs. 3(a) and 3(a′)]. On the other hand, the imaginary part of K′ is similar to the real part of K-exc. For the case of $d = 20$ nm, this picture is repeated, although the amplitudes become more comparable [Figs. 3(b) and 3(b′)]. For $d = 7$ nm, optical responses associated with K-exc and K′-exc become similar [Figs. 3(c) and 3(c′)].

The results presented in Fig. 3 suggest that for specific values of d, the K′ valley becomes a conjugate system. Under these conditions, Im[$\rho^{K',K}_{-,0}$] becomes quite dispersive at a wavelength wherein Re[$\rho^{K',K}_{-,0}$] is maximum. This is in contrast to what is seen for the case of the K valley wherein maximum of Im[$\rho^{K}_{+,0}$] happens when the value of Re[$\rho^{K}_{+,0}$] becomes zero. Dispersive absorption features, similar to those predicted in Figs. 3(a′) and 3(b′), have been studied in atomic systems extensively in the past [42,43]. In such systems, however, normally one is required to prepare coherent conditions that allow quantum interference to suppress absorption while offering large refractive index. Different schemes, including employment of three-level systems with use of an auxiliary field, have been used to prepare atomic systems for zero absorption with a high refractive index [19]. Such processes have also been studied in three-level intersubband systems in quantum wells [44,45]. The results presented in Fig. 3, however, suggest a different picture wherein no auxiliary field is needed. Instead, the zero-absorption with high refractive index is generated by a circularly polarized light in the K′ valley. The dispersive feature seen in Figs. 3(a′) and 3(b′) may be associated with the competition between GWI and absorption driven by the quantum interference effects, although in a system quite different from atomic systems [46].

The results for the real and imaginary parts of the normalized Rabi frequency and $\rho^{K'}_{-,-}$ in the K′ valley are shown in Fig. 4 (circles). For very large d, wherein the impact of the plasmon is ignorable, i.e., $\Omega^{K}_{nor} \sim \Omega^{K}_{0}$, we expect Ω^{K}_{nor}

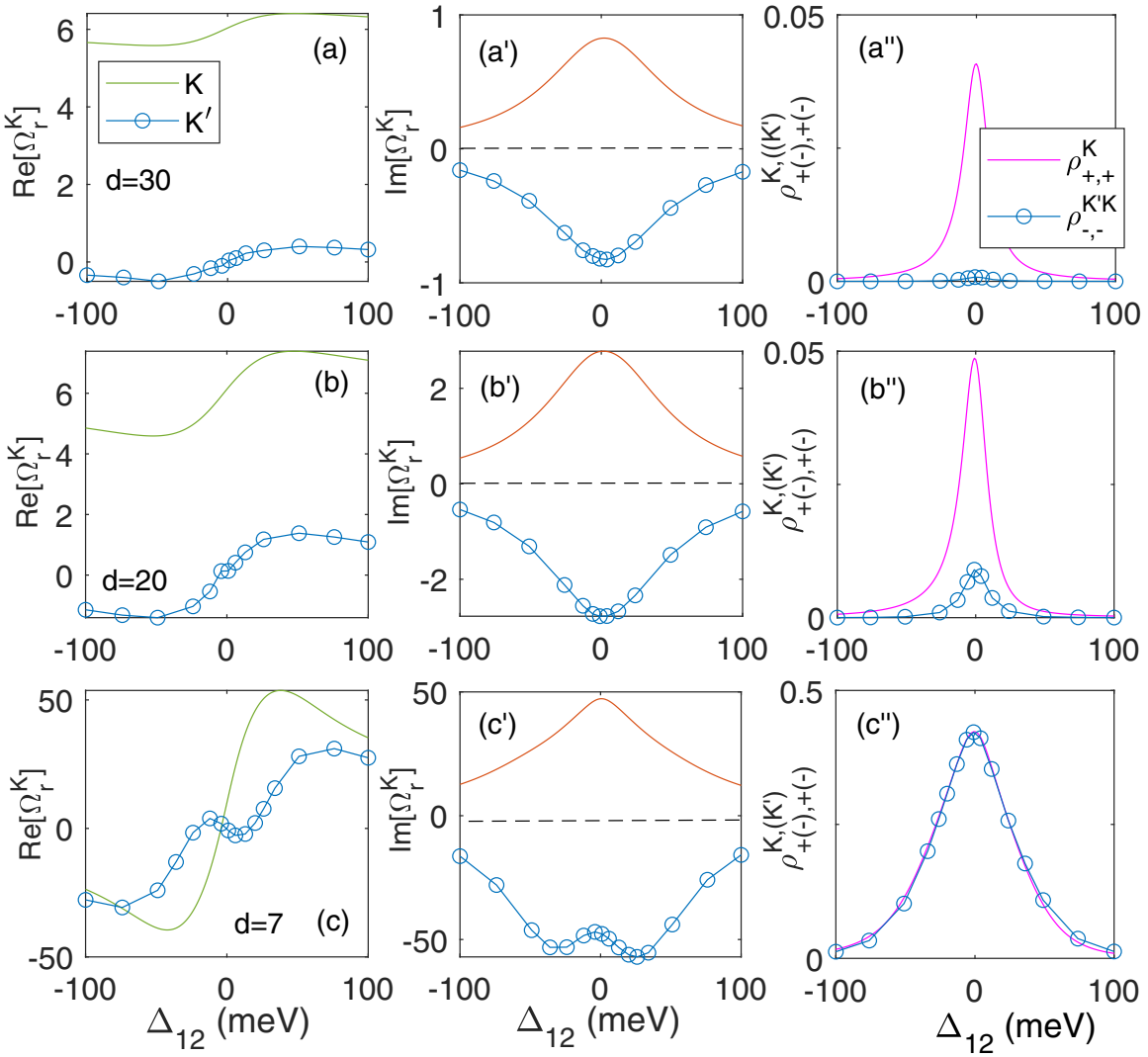

FIG. 4. Variations of $\mathrm{Re}[\Omega_r^{K,K'}]$ (a)–(c), $\mathrm{Im}[\Omega_r^{K,K'}]$ (a′)–(c′), and $\rho^K_{+,+}$ and $\rho^{K',K}_{-,-}$ (a″)–(c″) as a function of the laser frequency (Δ_{12}) when $d = 30$ (a), 20 (b), and 7 nm (c). All specifications are the same as those in Fig. 2.

to be real and $\Omega^{K',K}_{\mathrm{nor}} = 0$. As d becomes smaller, however, $\Omega^{K',K}_{\mathrm{nor}}$ starts to rise while $\Omega^{K}_{\mathrm{nor}}$ becomes complex. Figures 4(a) and 4(a′) show that when $d = 30$ nm, the normalized Rabi frequencies become frequency dependent with significant differences in the K (solid lines) and K′ valleys (circles). The results indicate that $\mathrm{Re}[\Omega^K_{\mathrm{nor}}]$ and $\mathrm{Re}[\Omega^{K',K}_{\mathrm{nor}}]$ have similar functionalities up to $d = 20$ nm [Figs. 4(a) and 4(b)], although the former is much larger than the latter. For $d = 7$ nm, however, they become quite different [Fig. 4(c)]. On the other hand, $\mathrm{Im}[\Omega^K_{\mathrm{nor}}]$ and $\mathrm{Im}[\Omega^{K',K}_{\mathrm{nor}}]$ seem to have opposite signs [Figs. 4(a′) and 4(b′)] and comparable values. When $d = 7$ nm, however, $\mathrm{Im}[\Omega^{K',K}_{\mathrm{nor}}]$ forms a doublet around $\Delta_{12} = 0$ [Fig. 4(c′)]. Additionally, the results show that as d decreases the magnitudes of the real and imaginary parts of Ω^K_{nor} and $\Omega^{K',K}_{\mathrm{nor}}$ are increased. This again indicates the impact of plasmon near fields. These results indicate that the phases of effective electric fields that drive K and K′ valleys are quite different. Therefore, although the K′ valley is not directly excited by the laser, K′-exc can be driven by K-exc with certain phase relation.

The results in Figs. 4(a″)–4(c″) show variation of $\rho^K_{+,+}$ (solid lines) and $\rho^{K',K}_{-,-}$ (circles) as a function of Δ_{12} for $d =$ 30, 20, and 7 nm, respectively. The results show that for large d one expects to get a negligible value for $\rho^{K',K}_{-,-}$ [Fig. 4(a″)]. As d increases, $\rho^{K',K}_{-,-}$ (circles) starts to catch up with $\rho^K_{+,+}$ [Fig. 4(b″)]. For $d = 7$ nm they become similar. These results suggest coherent excitation of K′-exc via plasmonic intervalley coupling. They also show how enhancement of the normalized Rabi frequencies can lead to overall enhancement of the population of K-exc and K′-exc. It is important to emphasize that the population in the K′ valley ($\rho^{K',K}_{-,-}$) is the result of intervalley quantum coherent transfer.

IV. EVOLUTION OF BLOCH VECTORS

To further analyze the exciton states in the K and K′ valleys, we study the evolution of the Bloch vectors associated with these valleys as a function of Δ_{12}. For this, note that the density matrix in the K′ valley [Eqs. (7)–(9)] can be written as

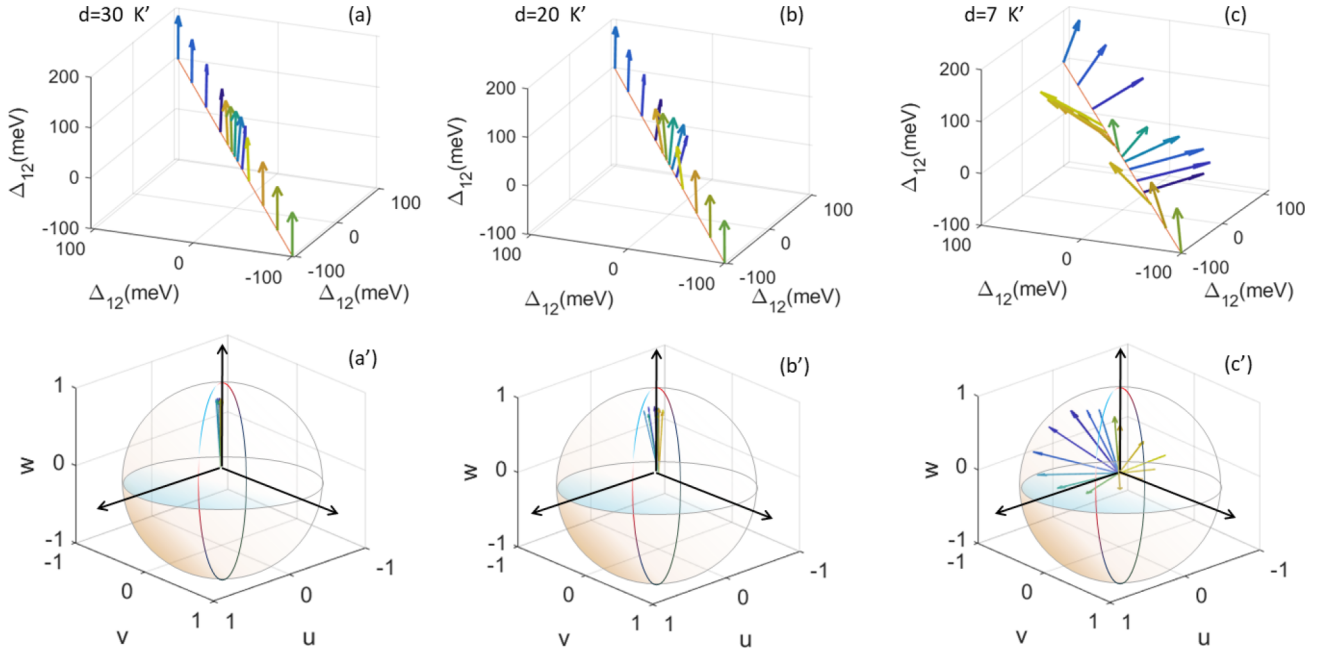

FIG. 5. Evolution of the Bloch vector associated with the K′ valley ($\mathbf{r}^{K',K}$) as a function of Δ_{12} for $d = 30$ (a), 20 (b), and 7 nm (c). (a′)–(c′) depict the dispersion of $\mathbf{r}^{K',K}$ in the Bloch sphere, respectively.

follows:

$$\rho^{K',K} = \begin{pmatrix} \cos^2\left(\frac{\theta}{2}\right) & e^{-i\phi}\cos\left(\frac{\phi}{2}\right)\sin\left(\frac{\theta}{2}\right) \\ e^{i\phi}\cos\left(\frac{\phi}{2}\right)\sin\left(\frac{\theta}{2}\right) & \sin^2\left(\frac{\theta}{2}\right) \end{pmatrix}. \quad (11)$$

Here

$$\phi = \tan^{-1}\left(\frac{\mathrm{Im}[\rho^{K',K}_{-,0}]}{\mathrm{Re}[\rho^{K',K}_{-,0}]}\right), \quad \theta = \cos^{-1}\left(\rho^{K',K}_{0,0} - \rho^{K'K}_{-,-}\right). \quad (12)$$

Considering these, the unit Bloch vector in the K′ valley is given by $\mathbf{r}^{K',K} = (u, v, w)$, wherein

$$u = \cos(\phi)\sin(\theta), \quad v = \sin(\phi)\sin(\theta), \quad w = \cos(\theta). \quad (13)$$

For the corresponding unit Block vector associated with the K valley ($\mathbf{r}^{K}$) we follow similar relations but using ρ^{K}.

The results in Figs. 5(a)–5(c) show the evolution of $\mathbf{r}^{K',K}$ as a function of Δ_{12}. Figure 5(a) shows that with the variation of Δ_{12}, the direction of $\mathbf{r}^{K',K}$ does not change significantly. This can be further seen in Fig. 5(a′), wherein we show this vector in the Bloch sphere. Lack of dispersion of this vector can be associated with the fact that the amount of coherently transferred excitation to K′ is not significant for $d = 30$ nm [Fig. 4(a″), circles]. For $d = 20$ nm, the situation is more or less similar, except for Δ_{12} close to zero, wherein we see a ripple in the direction of $\mathbf{r}^{K',K}$ [Fig. 5(b)]. This leads to some limited amount of spread in the Bloch sphere [Fig. 5(b′)]. The reason for the ripple can be found in the results for $\rho^{K',K}_{-,-}$ shown in Fig. 4(b″), wherein we see a rise in the value of this parameter around $\Delta_{12} \sim 0$. For $d = 7$ nm, the situation changes dramatically. Here we can clearly see strong variation of $\mathbf{r}^{K',K}$ with Δ_{12} [Fig. 5(c)] and its significant dispersion in the Bloch sphere [Fig. 5(c′)]. Note that these results show that a quarter of the Bloch sphere, bounded by $u = \{-1, +1\}$ and $w = \{0, 1\}$, is the accessible region for $\mathbf{r}^{K',K}$.

The vectors seen in Fig. 5 are color coded based on the values of the K′ valley polarization phase or ϕ [Eq. (12)]. This plays an important role in distinguishing the unique features of the K and K′ valleys. To explain this, in Fig. 6 we plot variations of ϕ as a function of Δ_{12} (circles) for the case of Fig. 5(c), i.e., $d = 7$ nm. Figure 6 also shows the projection of the Bloch vectors seen in Fig. 5(c) on the plane defined by the horizontal axes of this figure. The purpose of Fig. 6 is to show the correlation between the color of each vector and with the value of ϕ for different values of Δ_{12}. The results of this figure allow one to allocate certain phase information with the Bloch vectors shown in Fig. 5. Positive ϕ's are indicated with greenish colors, while negative ϕ's are indicated with bluish

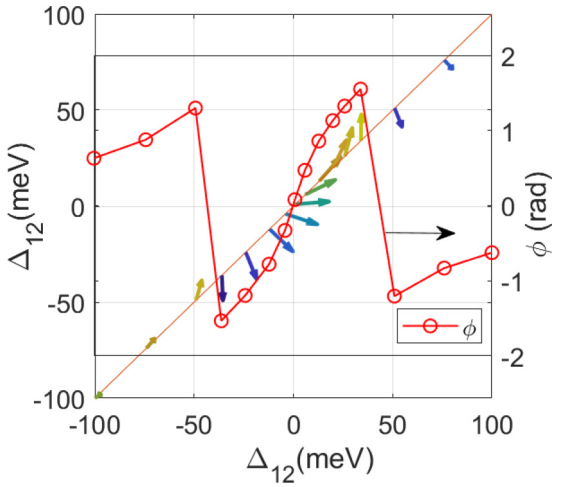

FIG. 6. Projection of the Bloch vectors shown in Fig. 5(c) on the plane defined by its horizontal axes. Circles show the values of ϕ as a function of Δ_{12}.

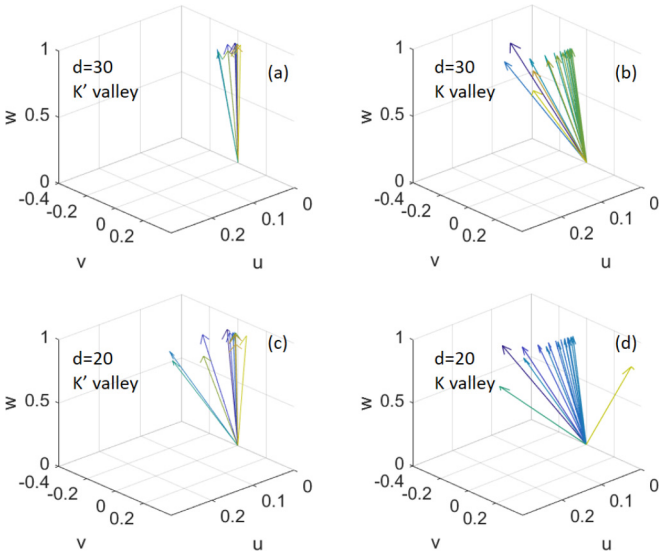

FIG. 7. Close views of dispersion of $\mathbf{r}^{K',K}$ [(a), (c)] and $\mathbf{r}^{K}$ [(b), (d)] under the same conditions as Fig. 5 for $d = 30$ [(a), (b)] and $d = 20$ nm [(c), (d)].

colors. Large negative values lead to darker blue and large positive values adopt pear color.

Figure 7 shows close views of the spread of $\mathbf{r}^{K}$ and $\mathbf{r}^{K',K}$ for $d = 30$ nm [Figs. 7(a) and 7(b)] and $d = 20$ nm [Figs. 7(a′) and 7(b′)] as Δ_{12} is varied. The results show that in the case of K′ valley [Figs. 7(a) and 7(c)], the dispersion of $\mathbf{r}^{K',K}$ seems to be far less than the case of $\mathbf{r}^{K}$ [Figs. 7(b) and 7(d)]. This is simply the result of higher population excitation in the case of K valley which increases the values of W. Additionally, the spread of $\mathbf{r}^{K',K}$ seems to more symmetric than that of $\mathbf{r}^{K}$. This can be related to the fact that K′ valley polarization for $\Delta > 0$ meV is closely conjugate of polarization for $\Delta_{12} < 0$ meV. This feature happens much less in the case of K valley. For the case of $d = 7$ nm, the distinctive features of $\mathbf{r}^{K',K}$ and $\mathbf{r}^{K}$, as expected from Figs. 3(c) and 3(c′).

V. CONCLUSIONS

We studied state of polarization of excitons in K and K′ valleys in a system consisting of a WS_2 ML and a Ag mANT. The results showed that when such a system interacts with a laser field that selectively excites K valley (σ_+ polarization), the coherent intervalley exciton-plasmon coupling and quantum coherence transfer can transform the K′ valley into a conjugate system. In such a system, the real and imaginary parts of the polarization behave as imaginary and real parts of polarization in the K valley, respectively. We showed formation GWI as the primary property of the K′ valley in the absence of the standard requirement of coherent preparation. The Bloch vectors associated with K and K′ valleys depict different phase information.

ACKNOWLEDGMENTS

This work is supported by the US National Science Foundation under Grant No. ECCS-1917544. J.Z.W. acknowledges support in part by US NSF Contracts No. NSF-DMR-1508494, No. NSF-ECCS-1809293, and No. NSF-DMR-1909292.

[1] T. Chervy, S. Azzini, E. Lorchat, S. Wang, Y. Gorodetski, J. A. Hutchison, S. Berciaud, T. W. Ebbesen, and C. Genet, ACS Photonics **5**, 1281 (2018).
[2] A. Boulesbaa, V. E. Babicheva, K. Wang, I. I. Kravchenko, M.-W. Lin, M. Mahjouri-Samani, C. B. Jacobs, A. A. Puretzky, K. Xiao, I. Ivanov *et al.*, ACS Photonics **3**, 2389 (2016).
[3] M.-E. Kleemann, R. Chikkaraddy, E. M. Alexeev, D. Kos, C. Carnegie, W. Deacon, A. C. Pury, C. Grose, B. Nijs, J. Mertens *et al.*, Nat. Commun. **8**, 1296 (2017).
[4] D. Zheng, S. Zhang, Q. Deng, M. Kang, P. Nordlander, and H. Xu, Nano Lett. **17**, 3809 (2017).
[5] W. Liu, B. Lee, C. H. Naylor, H.-S. Ee, J. Park, A. C. Johnson, and R. Agarwal, Nano Lett. **16**, 1262 (2016).
[6] X. Liu, W. Bao, Q. Li, C. Ropp, Y. Wang, and X. Zhang, Phys. Rev. Lett. **119**, 027403 (2017).
[7] J. Cuadra, D. G. Baranov, M. Wersall, R. Verre, T. J. Antosiewicz, and T. Shegai, Nano Lett. **18**, 1777 (2018).
[8] S. Wang, S. Li, T. Chervy, A. Shalabney, S. Azzini, E. Orgiu, J. A. Hutchison, C. Genet, P. Samori, and T. W. Ebbesen, Nano Lett. **16**, 4368 (2016).
[9] X. Han, K. Wang, P. D. Persaud, X. Xing, W. Liu, H. Long, F. Li, B. Wang, M. R. Singh, and P. Lu, ACS Photonics **7**, 562 (2020).
[10] Z. Li, Y. Xiao, Y. Gong, Z. Wang, Y. Kang, S. Zu, P. M. Ajayan, P. Nordlander, and Z. Fang, ACS Nano **9**, 10158 (2015).
[11] Y. Luo, C. Chi, M. Jiang, R. Li, S. Zu, Y. Li, and Z. Fang, Adv. Opt. Mater. **5**, 1700040 (2017).
[12] S.-H. Gong, F. Alpeggiani, B. Sciacca, E. C. Garnett, and L. Kuipers, Science **359**, 443 (2018).
[13] Z. Li, Y. Li, T. Han, X. Wang, Y. Yu, B. Tay, Z. Liu, and Z. Fang, ACS Nano **11**, 1165 (2017).
[14] Z. Li, C. Liu, X. Rong, Y. Luo, H. Cheng, L. Zheng, F. Lin, B. Shen, Y. Gong, S. Zhang *et al.*, Adv. Mater. **30**, 1801908 (2018).
[15] M. Alamri, B. Liu, S. M. Sadeghi, D. Ewing, A. Wilson, J. L. Doolin, C. L. Berrie, and J. Wu, ACS Appl. Nano Mater. **3**, 7858 (2020).
[16] S. A. Ghopry, M. Alamri, R. Goul, B. Cook, S. M. Sadeghi, R. R. Gutha, R. Sakidja, and J. Z. Wu, ACS Appl. Nano Mater. **3**, 2354 (2020).
[17] S. A. Ghopry, S. M. Sadeghi, Y. Farhat, C. L. Berrie, M. Alamri, and J. Z. Wu, ACS Appl. Nano Mater. **4**, 2941 (2021).
[18] S. M. Sadeghi and J. Z. Wu, ACS Photonics **6**, 2441 (2019).
[19] M. Fleischhauer, C. H. Keitel, M. O. Scully, C. Su, B. T. Ulrich, and S.-Y. Zhu, Phys. Rev. A **46**, 1468 (1992).
[20] M. D. Frogley, J. Dynes, M. Beck, J. Faist, and C. Phillips, Nat. Mater. **5**, 175 (2006).
[21] S. M. Sadeghi, J. Meyer, and H. Rastegar, Phys. Rev. A **56**, 3097 (1997).
[22] S. M. Sadeghi, J. F. Young, and J. Meyer, Phys. Rev. B **51**, 13349 (1995).

[23] S. G. Kosionis, A. F. Terzis, S. M. Sadeghi, and E. Paspalakis, J. Phys.: Condens. Matter **25**, 045304 (2012).
[24] M. A. Antón, F. Carreño, S. Melle, O. G. Calderón, E. Cabrera-Granado, and M. R. Singh, Phys. Rev. B **87**, 195303 (2013).
[25] S. Dufferwiel, T. Lyons, D. Solnyshkov, A. Trichet, A. Catanzaro, F. Withers, G. Malpuech, J. Smith, K. Novoselov, M. Skolnick *et al.*, Nat. Commun. **9**, 4797 (2018).
[26] G. Wang, X. Marie, B. L. Liu, T. Amand, C. Robert, F. Cadiz, P. Renucci, and B. Urbaszek, Phys. Rev. Lett. **117**, 187401 (2016).
[27] R. Schmidt, A. Arora, G. Plechinger, P. Nagler, A. G. Águila, M. V. Ballottin, P. C. Christianen, S. Michaelis de Vasconcellos, C. Schüller, T. Korn *et al.*, Phys. Rev. Lett. **117**, 077402 (2016).
[28] K. Hao, G. Moody, F. Wu, C. K. Dass, L. Xu, C.-H. Chen, L. Sun, M.-Y. Li, L.-J. Li, A. H. MacDonald *et al.*, Nat. Phys. **12**, 677 (2016).
[29] A. Hatef, S. M. Sadeghi, and M. R. Singh, Nanotechnology **23**, 205203 (2012).
[30] S. M. Sadeghi, A. Hatef, and M. Meunier, Appl. Phys. Lett. **102**, 203113 (2013).
[31] S. M. Sadeghi, W. J. Wing, and R. R. Gutha, Nanotechnology **26**, 085202 (2015).
[32] S. Dal Conte, F. Bottegoni, E. A. A. Pogna, D. De Fazio, S. Ambrogio, I. Bargigia, C. D'Andrea, A. Lombardo, M. Bruna, F. Ciccacci, A. C. Ferrari, G. Cerullo, and M. Finazzi, Phys. Rev. B **92**, 235425 (2015).
[33] C. R. Zhu, K. Zhang, M. Glazov, B. Urbaszek, T. Amand, Z. W. Ji, B. L. Liu, and X. Marie, Phys. Rev. B **90**, 161302(R) (2014).
[34] F. Bussolotti, H. Kawai, Z. E. Ooi, V. Chellappan, D. Thian, A. L. C. Pang, and K. E. J. Goh, Nano Futures **2**, 032001 (2018).
[35] M. R. Singh and P. D. Persaud, J. Phys. Chem. C **124**, 6311 (2020).
[36] J. D. Cox, M. R. Singh, C. Von Bilderling, and A. V. Bragas, Adv. Opt. Mater. **1**, 460 (2013).
[37] D. Erkensten, S. Brem, and E. Malic, Phys. Rev. B **103**, 045426 (2021).
[38] M. Selig, G. Berghäuser, A. Raja, P. Nagler, C. Schüller, T. F. Heinz, T. Korn, A. Chernikov, E. Malic, and A. Knorr, Nat. Commun. **7**, 13279 (2016).
[39] K. M. McCreary, M. Currie, A. T. Hanbicki, H.-J. Chuang, and B. T. Jonker, ACS Nano **11**, 7988 (2017).
[40] A. Laturia, M. L. Van de Put, and W. G. Vandenberghe, npj 2D Mater. Appl. **2**, 6 (2018).
[41] B. Zhu, X. Chen, and X. Cui, Sci. Rep. **5**, 9218 (2015).
[42] M. O. Scully, Phys. Rev. Lett. **67**, 1855 (1991).
[43] N. A. Proite, B. E. Unks, J. T. Green, and D. D. Yavuz, Phys. Rev. Lett. **101**, 147401 (2008).
[44] S. M. Sadeghi, H. M. van Driel, and J. M. Fraser, Phys. Rev. B **62**, 15386 (2000).
[45] Z. Wang, B. Yu, S. Zhen, and X. Wu, J. Lumin. **134**, 272 (2013).
[46] G. Grynberg and C. Cohen-Tannoudji, Opt. Commun. **96**, 150 (1993).